Research Article

Effect of Bedding Angle and Confining Pressure on the Brittleness of Geomaterials: A Case Study on Slate

Xianjie Hao [1,2,3,4,5] **Quansheng Xu,[5] Dequan Yang,[5] Shaohua Wang,[5] and Yingnan Wei[5]**

[1]*State Key Laboratory of Coal Resources and Safe Mining, China University of Mining and Technology (Beijing), Beijing 100083, China*
[2]*State Key Laboratory of Water Resource Protection and Utilization in Coal Mining, Beijing 100011, China*
[3]*Key Laboratory of Safety and High-efficiency Coal Mining, Ministry of Education (Anhui University of Science and Technology), Huainan 232001, China*
[4]*China University of Mining and Technology (Beijing), Beijing Laboratory of Companion Energy Accurate Mining, Beijing 100083, China*
[5]*School of Energy and Mining, China University of Mining and Technology (Beijing), Beijing 100083, China*

Correspondence should be addressed to Xianjie Hao; haoxianjie@cumtb.edu.cn

Brittleness is one of the most significant properties of geomaterials. However, very few studies have been conducted on factors influencing the rock brittleness indices. In this paper, conventional triaxial compression tests were carried out to investigate the effects of confining pressure and bedding angle on the brittleness of slate. From the perspective of energy, brittleness is an index that could reflect the release rate of energy that accumulated in the slate under the effect of external energy after reaching peak strength. Therefore, a new brittleness index of slate based on postpeak energy release is proposed herein. The applicability of this index is illustrated by comparing with other five existing brittleness indices. The following results can be obtained. (1) The confining pressure exerts a great influence on the brittleness of slate. With the increase of confining pressure, the brittleness of slate decreases significantly. The dispersion of brittleness values of slate declines with increasing confining pressure. (2) There is a parabolic relationship between slate brittleness and bedding angle. As bedding angle increases, the brittleness is intensified and reaches its maximum at a bedding angle of about 45° and then decreases gradually. (3) In contrast to the previous indices, the brittleness index proposed in this paper can describe the whole process of the postpeak stage through an index of the energy release, which makes this measure more suitable for rock that has the characteristics of step-drop or bench-drop at the postpeak stage.

1. Introduction

Brittleness is one of the most significant mechanical properties of geological materials [1]. On the one hand, brittleness indices are widely used in rock engineering. For instance, rock brittleness is used to characterize the rock drilling performance during the tunnelling excavation process using a TBM [2, 3]; shale brittleness is utilized to evaluate the mechanical properties and fracturing effects of shale gas reservoirs [4, 5]. In addition, some brittle rock, such as granite, has outstanding applications in geological engineering due to its stability [6]. The thick granite layer in

Beishan, China, was chosen as the underground nuclear waste disposal base [7, 8], and the underground laboratory of Atomic Energy Canada Limited was also constructed in a granite layer [9, 10]. On the other hand, the failure process of brittle rock generally releases a lot of energy and leads to dynamic disasters in rock engineering. For instance, the failure of brittle rock in deep underground excavation projects regularly triggers rockbursts [11, 12], and the mining process in deep coal mines with hard surrounding rock might induce coal bumps [13, 14].

The research on the rock brittleness has significance in rock engineering. Generally speaking, rock brittleness is a

concept contrary to rock plasticity, referring to rock fractures at or slightly beyond the yield stress. To characterize rock brittleness, a number of brittleness indices have been proposed. These main brittleness indices can be divided into the following three types, respectively, based on the strength parameters [15–19], deformation parameters [15, 20–22], and energy parameters [23–26]. Among these indices, brittleness indices based on strength and deformation parameters have a shortcoming, i.e., these indices fail to define the rock scale from brittleness to ductility [26]. In contrast, brittleness indices based on energy parameters are gaining popularity for the conciseness. In general, the aforementioned criteria have observably promoted research into rock brittleness; however, research into the factors influencing rock brittleness indices is insufficient. In respect to confinement, some scholars [27, 28] characterized the strength of intact brittle rock considering confinement using an s-shaped failure criterion highlighting the transition of failure modes, while the research [29] revealed the brittle behavior of soft calcarenites under low confinement regimes [30]. The drained triaxial tests were conducted on Beaucaire marl under a wide range of confining pressure and the brittle-to-ductile transition was described [30]. A study [31] investigated the effect of bedding structure on the brittle failure of deep shale. In addition, an evaluation method for the strength and failure of brittle rock containing initial cracks was proposed [32]. Besides, [33] the effect of porosity on rock brittleness was investigated.

The statement above indicates that there are very few studies considering the factors influencing the rock brittleness indices. There are bedding planes in rock mass related to geotechnical engineering operations and there are different confining pressures acting on the surrounding rocks in underground engineering works. Laboratory tests, including triaxial compression tests [34], acoustic emission tests [35], indentation tests [36], and numerical simulations [37, 38], show that bedding angle and confining pressure directly affect the mechanical behavior of rock, such as its strength and failure mode. The study of the influence of bedding angle and confining pressure on brittleness has certain significance for supporting design of rock slopes and underground tunnels, quantitative evaluation of surrounding rock stability, and installation of pipelines and installation of pipelines and conduits in shallow formations [38, 39]. Bedding angle and confining pressure have a significant influence on the brittleness of rock; however, there is a lack of research into the brittleness of rocks due to bedding angle and confining pressure. Therefore, it is valuable to study the influence of bedding angle and confining pressure on brittleness.

In this paper, conventional triaxial compression tests were conducted to investigate the effects of confining pressure and bedding angle on the brittleness of slate. In the second section, the preparation of the specimens and the test processes are introduced. In the third section, the experimental results under different confining pressures and bedding angles are demonstrated. In the fourth section, a new brittleness index of slate based on postpeak energy release is presented. The effects of confining pressure and bedding angle on the brittleness of slate are analyzed by using the new brittleness index in this section. In the fifth section, the applicability of the index proposed by this paper is illustrated by comparison with five existing brittleness indices. The new brittleness index based on energy release is of great significance to the quantitative evaluation of surrounding rock stability.

2. Experimental Setup

2.1. Site Sampling. In order to demonstrate the influences of bedding and confining pressure on the brittleness of rock, the selected rock specimens should have a developed bedding structure and relatively high brittleness. So, slate was selected as the research sample in this case. According to the sampling situation in the field (Figure 1), the sample is a sandy slate. The selected sample is composed of detritus and limestone. In the sample, there is a porous form of cementation, which is mainly composed of siliceous matter, calcium carbonate, clay, iron oxide, calcium sulphates, etc. Testing showed that the slate has a loose structure and poor weathering and water resistance. Through scanning electron microscopy and by extracting salient microcrack parameters of specimens, it is found that the microcrack area ratio of these specimens in a direction parallel to the bedding plane is between 0.024 and 0.036, and the microcrack area ratio normal to the bedding plane is between 0.034 and 0.051 [40], which indicates that the microcrack density dispersion of these specimen is small and has good consistency.

2.2. Test Scheme. To study the influences of bedding and confining pressure on the brittleness of slate, it is necessary to obtain the complete stress-strain curves of slate under different bedding angles and confining pressures. The confining pressures were set to 0 MPa, 10 MPa, 20 MPa, 40 MPa, and 60 MPa: the bedding angles were set to 0°, 15°, 30°, 45°, 60°, 75°, and 90°. The experimental scheme is illustrated in Figure 2.

2.3. Preparation of Specimens with Different Bedding Angles. The specific preparation steps of slate specimens with different bedding angles are as follows:

(1) Firstly, the bulk rock specimens were placed on a workbench, and then the dip direction and dip angle (φ) of the sample were measured with a geological compass. After that, the slate specimens were correspondingly rotated in the vertical plane where the dip direction was located (the rotation angle is $-\varphi$). Then the rotated rock specimens were fixed by using clamping device; then the bottom surface of the rock sample was flattened by a mechanical grindstone. Then the dip direction and dip angle (φ) of the sample were measured again with the geological compass. The specimens were rotated and flattened again if the bedding angle is greater than 1°. Thus, slate specimens with horizontal bedding were obtained.
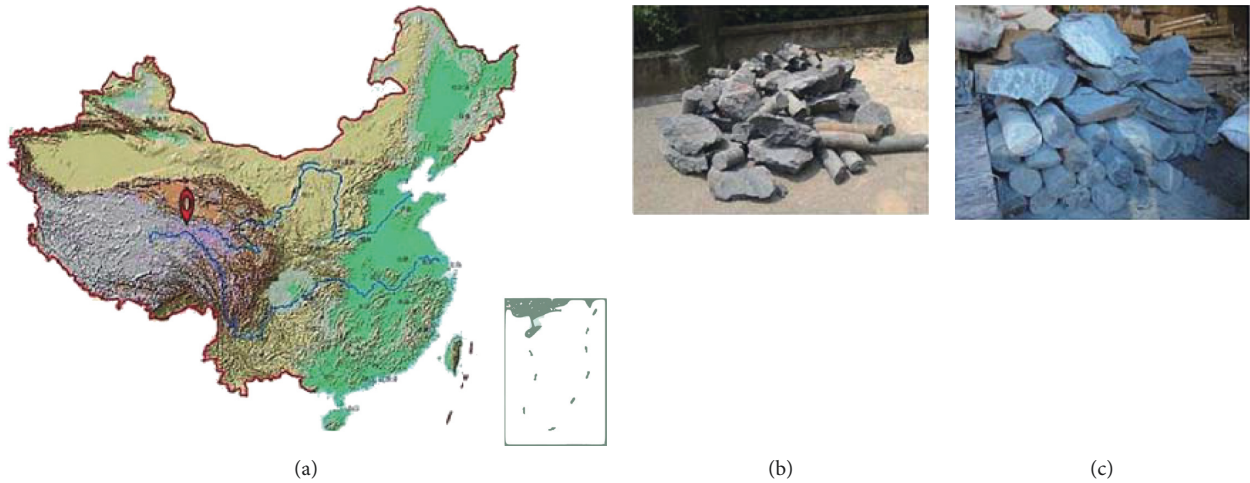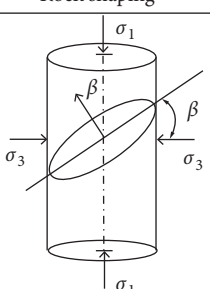
(a) (b) (c)

FIGURE 1: Rock sample acquisition site and sampling.

Rock shaping	Confining pressure, angle of bedding				
	Confining pressure (MPa)				
	0, 0	0, 10	0, 20	0, 40	0, 60
	15, 0	15, 10	15, 20	15, 40	15, 60
	30, 0	30, 10	30, 20	30, 40	30, 60
	45, 0	45, 10	45, 20	45, 40	45, 60
	60, 0	60, 10	60, 20	60, 40	60, 60
	75, 0	75, 10	75, 20	75, 40	75, 60
	90, 0	90, 10	90, 20	90, 40	90, 60

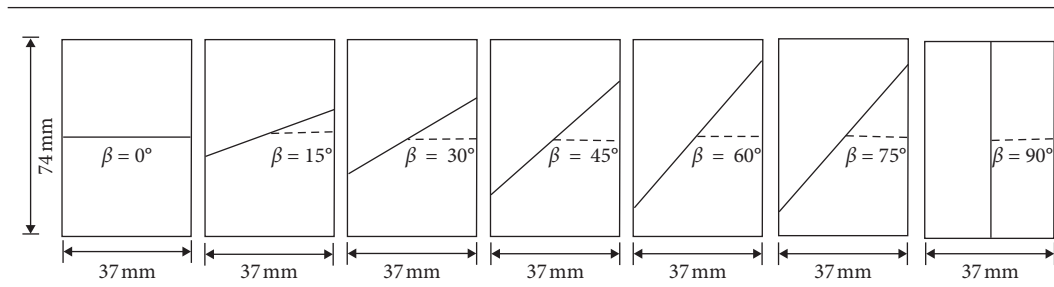FIGURE 2: Diagram of confining pressure and bedding arrangements.

(2) The slate specimens obtained in Step (1) were placed on the working platform of drilling machine. As shown in Figure 3(a), the bedding angle of the sample was adjusted so that the true dip angle is equal to the designed angle β, as shown in Figure 2.

(3) The rotated rock specimens were then fixed using a clamping device to ensure that there was no sliding in the sample-drilling process. The specimen preparation and triaxial compression tests should indeed refer to the ISRM standard (φ 50 mm $\times$ 100 mm); however, due to the significant influence of the bedding planes during slate processing, the specimens are often badly damaged. According to the results of Yang et al. [41], the triaxial compression strength of rock specimens measuring φ 37 mm $\times$ 74 mm is slightly different from

that at φ 37 mm $\times$ 74 mm; therefore, a core-drill with an internal diameter of 37 mm was used to drill the specimens as shown in Figure 3(b). A number of cylindrical cores with a diameter of 37 mm and bedding angle β were obtained as shown in Figures 3(c) and 3(d).

(4) The true dip angle of the bedding of sample was adjusted and Steps (2) and (3) were repeated. Finally, all the specimens with bedding angles of 0°, 15°, 30°, 45°, 60°, 75°, and 90° were acquired: the number of cores with each bedding angle was no less than 12.

(5) These cores were trimmed and sliced to cylinders with a height of 74 mm, as shown in Figure 3(e). According to the ISRM suggested method for preparing specimens for conventional triaxial compression testing,
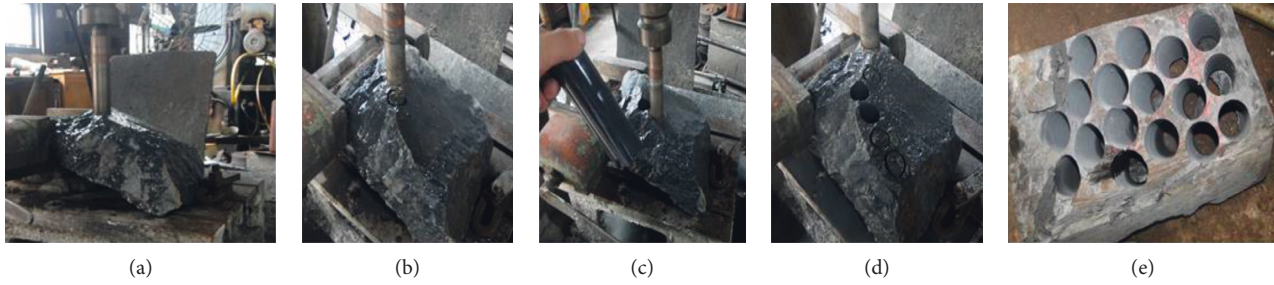
(a)   (b)   (c)   (d)   (e)

FIGURE 3: The preparation of specimens.

the two ends of each specimen were ground to ensure that both planes are horizontal within accuracy of ±0.05 mm and perpendicular to the longitudinal axis within ±0.25°.

2.4. Experimental Apparatus. The triaxial quasistatic compression test was carried out using an MTS815.03 testing machine (MTS Corporation, USA). It is mainly used for mechanical tests of materials such as rock and concrete. It is equipped with a servocontrolled, fully automatic, triaxial pressurization and measurement system (Figure 4). An axial force up to 4600 kN and a confining pressure of up to 140 MPa can be applied.

The experimental process is as follows:

(1) The prepared rock specimens are numbered one by one with the format sample of "β–n," where β represents the bedding angle of specimen, n denotes the number of specimens.

(2) After measuring the size of the specimens, it was placed in the loading chamber. The axial displacement sensors and the circumferential displacement sensors were installed.

(3) The control mode is displacement-controlled: specimens were loaded at a rate of 0.01 mm/s. The predetermined initial confining pressure (0, 10, 20, 40, and 60 MPa) was applied progressively as a static hydraulic pressure. During the loading process, the data sampling frequency was 2 Hz. The specimens were loaded until they were destroyed. During the experiment, the data were collected automatically and the complete stress-strain curves were drawn.

(4) After the specimen was destroyed, the test was stopped, the specimen was removed, and the form of destruction of the specimen was recorded and described.

3. Test Results

Some 74 slate specimens were successfully tested in conventional triaxial compression experiments. A three-dimensional scatter plot of the relationship between compressive strength, confining pressure, and bedding angle is shown in Figure 5: the compressive strength increases linearly with increasing confining pressure. The typical stress-strain curves of these specimens are shown in Figures 6–10.
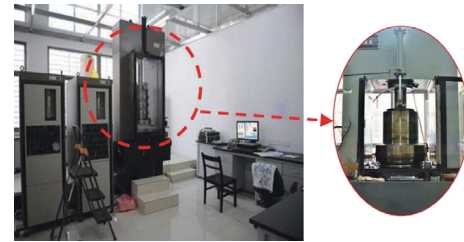

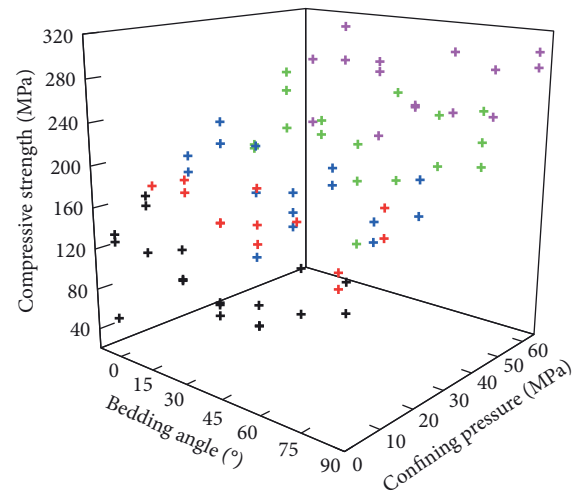FIGURE 4: Experimental apparatus.

FIGURE 5: A three-dimensional scatter plot of the relationship between compressive strength, confining pressure, and bedding angle.

It can be seen from Figures 6–10, that the stress and strain curves of slab rock are affected by confining pressure and bedding angle. The compressive strength is enhanced with the increase in confining pressure. The slate stress-strain curves show different ways of falling at the postpeak stage. Some curves exhibit direct drops, as shown in specimen 0-3 (bedding angle, 0°): some curves drop by one level, as shown in specimen 30-1 (bedding angle, 0°). There are also specimens showing multiple steps, as shown in specimen 75-5 (bedding angle, 75°). It can be seen that the shape of the postpeak curve varies under different bedding angles. In summary, the slate stress-strain curve is affected by confining pressure and bedding angle both at the prepeak stage and the postpeak stages. The brittleness is
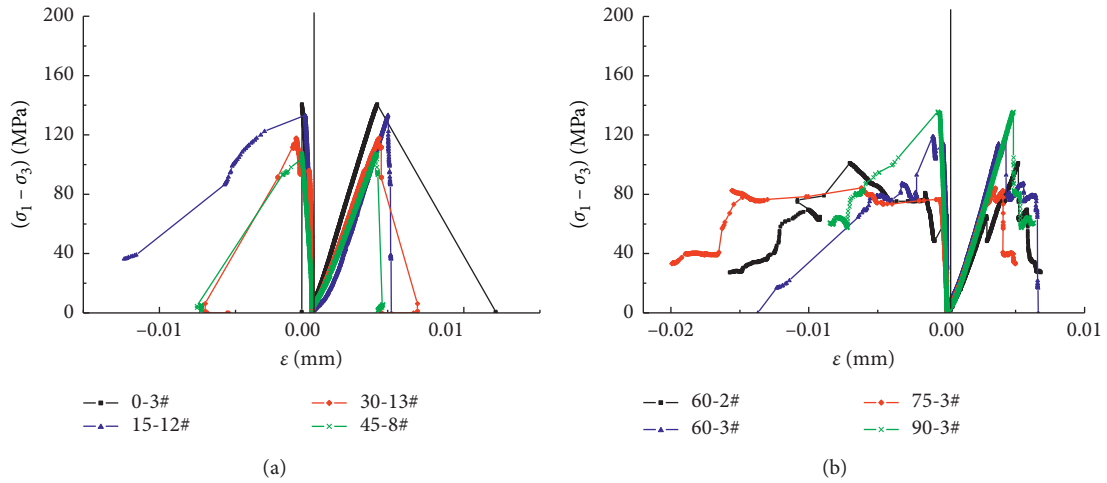
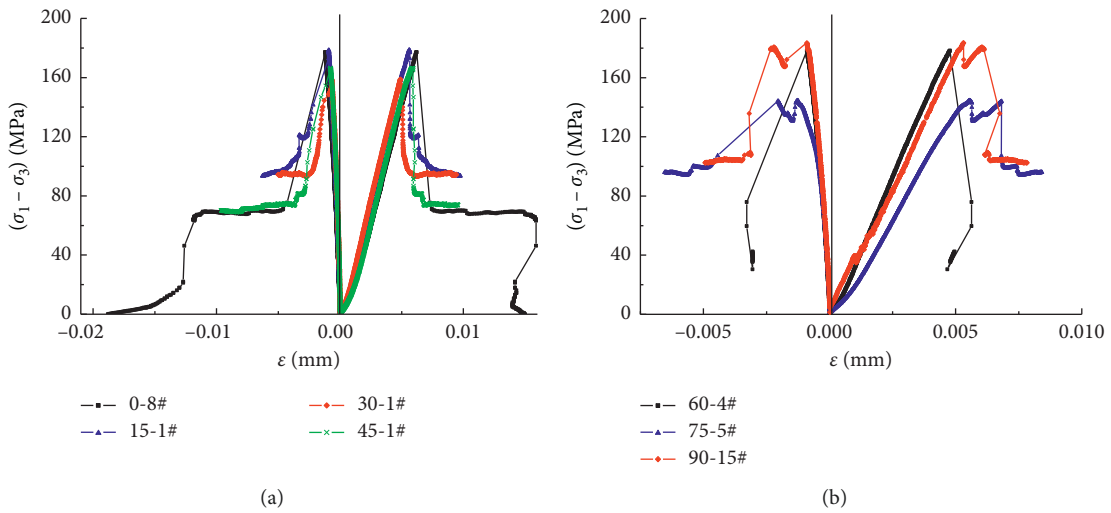FIGURE 6: The stress-strain curves of the specimens: confining pressure of 0 MPa.

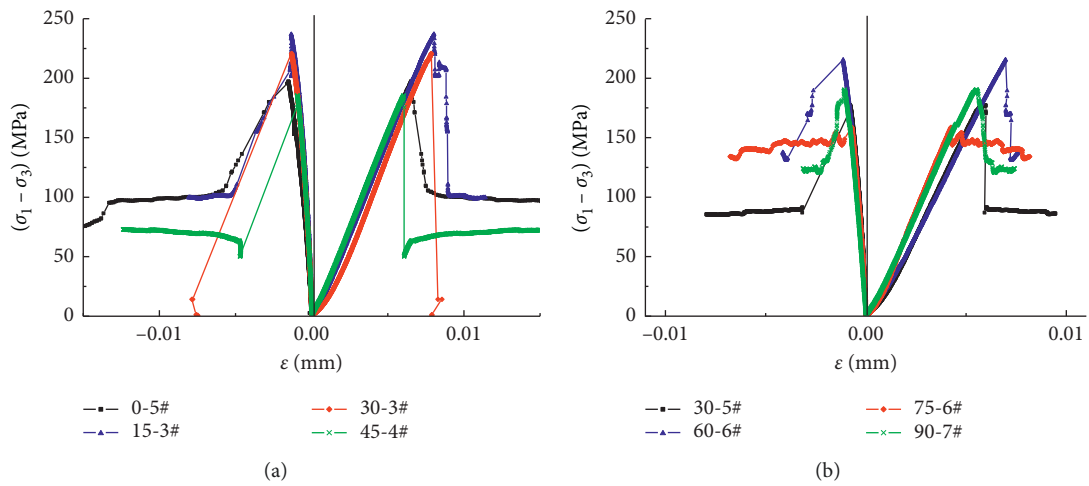FIGURE 7: The stress-strain curves of the specimens: confining pressure of 10 MPa.

FIGURE 8: The stress-strain curves of the specimens: confining pressure of 20 MPa.
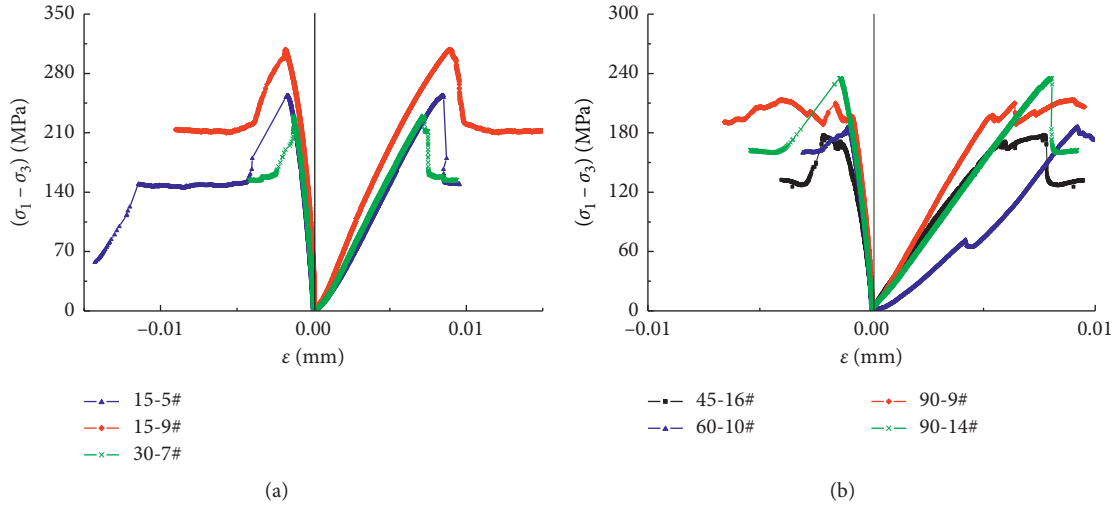
(a)

(b)

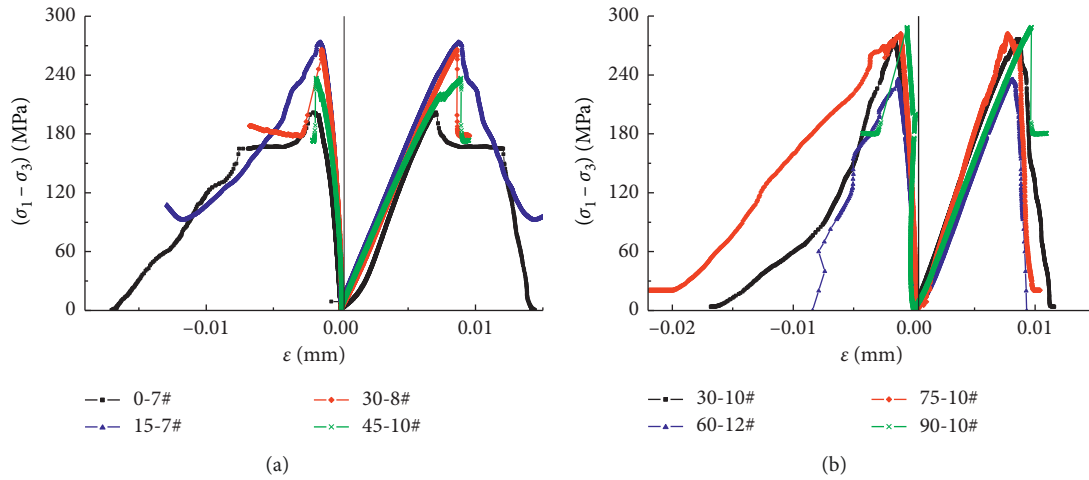FIGURE 9: The stress-strain curves of the specimens: confining pressure of 40 MPa.

(a)

(b)

FIGURE 10: The stress-strain curves of the specimens: confining pressure of 60 MPa.

also affected by confining pressure and bedding angle. Therefore, the study on the influences of confining pressure and bedding angle on the brittleness of slate is of significance during the excavation of this type of chamber in practical engineering works.

4. Effects of Confining Pressure and Bedding Angle on the Brittleness of Slate

4.1. A Brittleness Index Based on Postpeak Energy Release for Slate

4.1.1. Energy Accumulation at the Prepeak Stage. According to the law of conservation of energy, the amount of work done by an external force on an object is equal to the amount of energy change in the object:

$$W = \Delta U, \qquad (1)$$

where W is the amount of the work done by the external force on the object, and ΔU represents the amount of the energy change in the object.

Energy accumulation mainly occurs in the prepeak stage of the stress-strain curve of slate subjected to conventional triaxial compression:

$$W_{\text{mf·A}} = \Delta U_{\text{sf·A}} = V \cdot \int_0^{\varepsilon_{\text{A·P}}} S_{(\text{A})} d\varepsilon,$$

$$W_{\text{mf·C}} = \Delta U_{\text{sf·C}} = V \cdot \sigma_{\text{C}} \cdot \varepsilon_{\text{C·P}}, \qquad (2)$$

where $W_{\text{mf·A}}$ is the energy accumulated at the axial prepeak stage in Figure 11, $W_{\text{mf·C}}$ refers to the energy accumulated at the circumferential prepeak stage in Figure 11, $\Delta U_{\text{sf·A}}$ is the increment of the axial strain energy at the prepeak stage in Figure 11, $\Delta U_{\text{sf·C}}$, represents the increment of the circumferential strain energy at the prepeak stage in Figure 11, V is the volume of the specimen, $S_{(\text{A})}$ is the axial stress-strain curve for slate, σ_{C} is the confining pressure, and $\varepsilon_{\text{C·P}}$ is the circumferential strain on the specimen at the peak stress.

Most of the work done by the external load before the peak strength is converted to strain energy of the specimens, and a small percentage of the work is converted to the energy dissipated in crack propagation and so on. Since slate is a
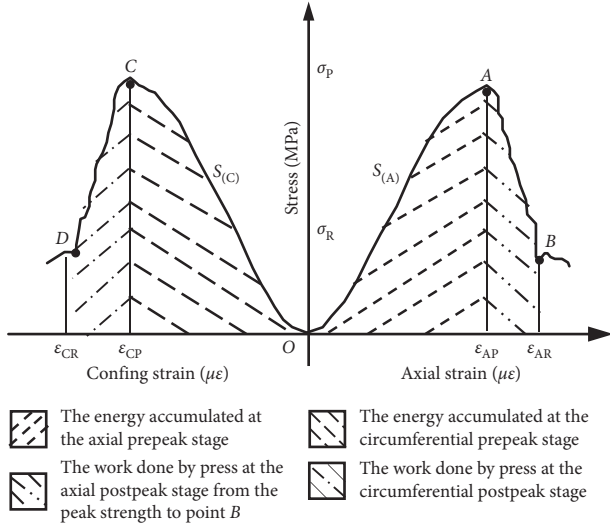
FIGURE 11: Schematic diagram of slate brittleness calculation.

hard rock, the uniaxial compressive strength of slate is usually over 100 MPa. According to the analysis of the stress-strain curves of the slate specimens, the stage of nonlinear elastic deformation and the plastic stage of the slate are both small. Therefore, the energy dissipation in the nonlinear elastic deformation and the plastic stages is not considered in the analysis of the brittleness index of slate. The total mechanical work done by the mechanical press W_{mf} is

$$W_{mf} = W_{mf \cdot A} + W_{mf \cdot C}, \tag{3}$$

$$W_{mf} = V \cdot \left(\int_0^{\varepsilon_{A \cdot P}} S_{(A)} d\varepsilon - \sigma_C \cdot \varepsilon_{C \cdot P} \right), \tag{4}$$

where W_{mf} is the energy accumulated at the prepeak stage.

4.1.2. Unsteady Dissipation of Energy at the Postpeak Stage.
The slate specimens were destroyed at postpeak stage, and the energy was released at this stage. The mechanical work done by the mechanical press was converted into dissipative energy at the postpeak stage. Besides this, the strain energy accumulated before reaching peak strength was also converted into dissipative energy until the residual stage. The mechanical work done by the press is

$$W_{mb \cdot A} = V \cdot \int_{\varepsilon_{A \cdot P}}^{\varepsilon_{A \cdot R}} S_{(A)} d\varepsilon,$$

$$W_{mb \cdot C} = V \cdot \sigma_C \cdot (\varepsilon_{C \cdot P} - \varepsilon_{C \cdot R}),$$

$$W_{mb} = W_{mb \cdot A} + W_{mb \cdot C} \tag{5}$$

$$= V \cdot \left(\int_{\varepsilon_{A \cdot P}}^{\varepsilon_{A \cdot R}} S_{(A)} d\varepsilon + \sigma_C \cdot (\varepsilon_{C \cdot P} - \varepsilon_{C \cdot R}) \right),$$

where $W_{mb \cdot A}$ is the work done by press at the axial postpeak stage from the peak strength to point B in the stress-strain curve, $\varepsilon_{A \cdot P}$ denotes the strain at point P, $W_{mb \cdot C}$ is the work done by press at the circumferential postpeak stage, and W_{mb} refers to the work done by the press in the postpeak stage.

The residual strain energy after the peak is

$$W_R = \left((\sigma_P + \sigma_C)^2 - \sigma_P^2 \right) / (2 \cdot E), \tag{6}$$

where W_R is the residual strain energy after the peak, E is the deformation modulus of the specimen, σ_P is the compressive strength, and σ_C represents the circumferential confining pressure.

From Equations (3), (5), and (6), the increment in dissipated energy after peak strength is

$$\Delta U_{db} = W_{mf} + W_{mb} - W_R, \tag{7}$$

where W_{mb} is the mechanical work done by the press at the postpeak stage in Figure 11.

4.1.3. A New Brittleness Index Based on the Unsteady Release of Energy.
The brittleness is an index that reflects the release rate of energy accumulated in the slate under the effect of external energy input after the peak strength from the perspective of energy, which is

$$Br = \frac{\Delta U_{db}}{W_{mb \cdot A}}, \tag{8}$$

where Br is the brittleness of slate, ΔU_{db} represents the increment of dissipation energy released at the postpeak stage, and W_{mb} denotes the mechanical work done by the press after reaching peak strength.

The brittleness of slate can be obtained from Equations (5), (7), and (8):

$$Br = \frac{\int_0^{\varepsilon_{A \cdot P}} S_{(A)} d\varepsilon + \sigma_C \cdot \varepsilon_{A \cdot P} - \left[\int_{\varepsilon_{A \cdot P}}^{\varepsilon_{A \cdot R}} S_{(A)} d\varepsilon + \sigma_C \cdot (\varepsilon_{C \cdot R} - \varepsilon_{C \cdot P}) \right] - \left[\left((\sigma_P + \sigma_C)^2 - \sigma_P^2 \right) / (2 \cdot E) \right]}{\int_{\varepsilon_{A \cdot P}}^{\varepsilon_{A \cdot R}} S_{(A)} d\varepsilon}. \tag{9}$$

4.2. Brittleness Calculation.
The brittleness indices of slate could be calculated by using Equation (9). The calculated results are displayed in Table 1.

4.3. Correlation Analysis of Brittleness and Confining Pressure.
A three-dimensional scatter diagram showing brittleness, confining pressure, and bedding angle is shown in Figure 12.

A fitting curve between brittleness and confining pressure is illustrated in Figure 13.

It can be seen that there is a negative correlation between the brittleness and the confining pressure from Figure 13. With the increase of confining pressure, the brittleness of slate decreases. The conclusion is consistent with the general understanding among current scholars. With the increase of confining pressure, there is a transition in the rock from

TABLE 1: The calculated slate brittleness indices.

Numbers	Energy accumulated at the axial prepeak stage (10^6 J/m^3)	Energy accumulated at the circumferential prepeak stage (10^6 J/m^3)	Work done by press tester at the axial postpeak stage (10^6 J/m^3)	Work done by press tester at the circumferential postpeak stage (10^6 J/m^3)	Residual strain energy (10^6 J/m^3)	Brittleness
0-1#	0.2927	0.0000	0.0000	0.0000	0.0000	5.6147
0-2#	0.2095	0.0000	0.1300	0.0000	0.0086	2.5450
0-3#	0.3059	0.0000	0.5504	0.0000	0.0000	1.5558
15-11#	0.5099	0.0000	0.2632	0.0000	0.2697	1.9124
15-12#	0.2853	0.0000	0.0181	0.0000	0.0000	16.7754
30-11#	0.2431	0.0000	0.0242	0.0000	0.0000	11.0322
30-13#	0.2596	0.0000	0.1332	0.0000	0.0000	2.9487
45-6#	0.2298	0.0000	0.1349	0.0000	0.0000	2.7034
45-7#	0.2008	0.0000	0.0405	0.0000	0.0142	5.6051
45-8#	0.2221	0.0000	0.0204	0.0000	0.0002	11.8561
60-1#	0.1822	0.0000	0.0310	0.0000	0.0000	6.8827
60-2#	0.2561	0.0000	0.0682	0.0000	0.0202	4.4588
60-3#	0.2573	0.0000	0.1847	0.0000	0.0000	2.3930
75-3#	0.1502	0.0000	0.0786	0.0000	0.0189	2.6709
90-1#	0.4136	0.0000	0.0140	0.0000	0.3559	5.1345
90-3#	0.3040	0.0000	0.0432	0.0000	0.0584	6.6838
0-8#	0.5707	0.0059	0.7587	0.0881	0.0036	1.6768
15-1#	0.5338	0.0045	0.4728	0.0269	0.1616	1.7538
15-2#	0.6155	0.0049	0.1168	0.0253	0.0462	5.0407
30-1#	0.4219	0.0034	0.1319	0.0081	0.1608	2.8893
30-2#	0.5412	0.0035	0.0154	0.0077	0.2033	15.7825
45-1#	0.5012	0.0039	0.1267	0.0144	0.1206	3.7246
45-2#	0.7414	0.0053	0.0181	0.0243	0.1103	15.9934
45-12#	0.4410	0.0052	0.1051	0.0127	0.1050	3.8964
60-4#	0.4670	0.0045	0.0741	0.0120	0.0609	5.7707
75-4#	0.2974	0.0055	0.0596	0.0094	0.0938	4.0332
75-5#	0.4557	0.0063	0.2694	0.0216	0.1993	1.9027
90-5#	0.7290	0.0079	0.0475	0.0253	0.1789	8.6697
90-15#	0.5098	0.0045	0.3157	0.0178	0.1813	1.9987
0-5#	0.7727	0.0152	0.2721	0.0432	0.2222	2.7943
0-9#	0.6931	0.0143	0.4624	0.0395	0.2382	1.9349
15-3#	1.1013	0.0135	0.3235	0.0387	0.2383	3.4198
15-4#	1.0216	0.0128	0.0951	0.0558	0.1516	6.8464
30-3#	0.9627	0.0132	0.0675	0.0650	0.0266	8.1641
30-4#	0.3269	0.0187	0.1497	0.0520	0.0748	2.3430
30-5#	0.6205	0.0078	0.3671	0.0529	0.1834	2.0591
45-3#	0.6600	0.0076	0.0685	0.0291	0.1357	6.4496
45-4#	0.5255	0.0095	0.1420	0.0398	0.1097	3.3396
45-13#	0.5825	0.0142	0.0508	0.0584	0.0100	6.3732
60-6#	0.8563	0.0114	0.0507	0.0277	0.3548	7.5410
60-7#	0.8656	0.0111	0.0224	0.0148	0.4713	11.8739
75-6#	0.3991	0.0070	0.5300	0.0044	0.3469	1.1107
75-7#	0.5409	0.0098	0.0965	0.0926	0.0792	3.4931
90-6#	0.9810	0.0145	0.1263	0.0325	0.2387	5.7626
90-7#	0.6370	0.0108	0.2139	0.0159	0.2754	2.6204
0-10#	0.8492	0.0262	0.2650	0.6138	0.0521	1.9369
15-5#	1.3897	0.0334	0.0554	0.0544	0.5681	8.7839
15-6#	1.1695	0.0256	0.2547	0.1320	0.2562	3.4277
15-9#	1.8193	0.0364	0.7406	0.0674	0.8540	2.2397
30-6#	1.1028	0.0245	0.2972	0.0327	0.5105	2.8697
30-7#	1.0334	0.0264	0.1070	0.0432	0.5571	4.3473
45-5#	0.4858	0.0328	0.0834	0.1437	0.0622	3.0100
45-14#	1.0787	0.0371	0.0695	0.0383	0.4270	7.3877
45-16#	1.1642	0.0427	0.1206	0.0202	0.5456	5.6984
60-8#	1.1881	0.0286	0.0645	0.0327	0.7086	6.2265
60-10#	1.0959	0.0206	0.3090	0.0272	0.9932	1.3665

TABLE 1: Continued.

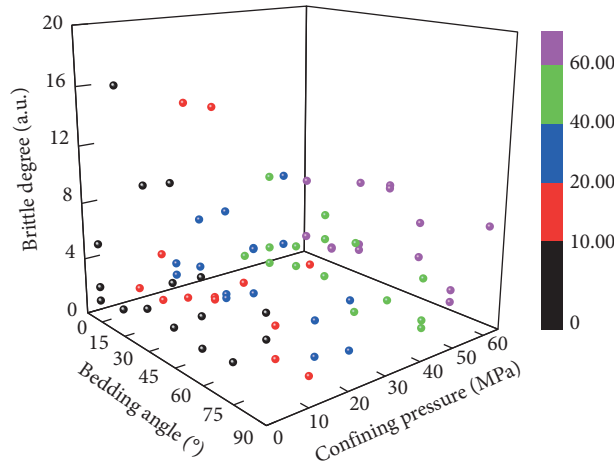| Numbers	Energy accumulated at the axial prepeak stage (10^6 J/m^3)	Energy accumulated at the circumferential prepeak stage (10^6 J/m^3)	Work done by press tester at the axial postpeak stage (10^6 J/m^3)	Work done by press tester at the circumferential postpeak stage (10^6 J/m^3)	Residual strain energy (10^6 J/m^3)	Brittleness
75-9#	0.9658	0.0254	0.1147	0.3107	0.0711	3.1626
90-8#	1.4660	0.0304	0.2457	0.0320	0.9974	2.7966
90-9#	1.6293	0.0809	0.4541	0.0447	1.0685	2.2866
90-14#	1.2778	0.0278	0.0828	0.0609	0.6480	5.5740
0-7#	1.5891	0.0568	0.8313	0.4532	0.1189	2.1887
0-11#	1.6423	0.0675	0.1200	0.0603	0.6735	6.7483
15-7#	1.8402	0.0450	1.2895	0.3018	0.3981	1.9346
15-8#	1.9970	0.0545	0.9092	0.1012	0.9924	2.0482
30-8#	1.6819	0.0429	0.0757	0.0432	0.9060	7.8858
30-9#	1.1487	0.1494	0.2745	0.2496	0.1915	3.1117
30-10#	1.7628	0.0473	0.5619	0.4387	0.1295	2.6797
45-10#	1.7374	0.0552	0.1132	0.0039	0.9310	8.3590
45-11#	1.5292	0.0542	0.0824	0.0047	1.0035	8.1359
60-11#	1.9065	0.0482	0.1345	0.0044	1.2486	6.3178
60-12#	1.4069	0.0400	0.2523	0.2120	0.1404	3.8142
75-10#	1.5023	0.0336	0.5206	0.5644	0.1481	2.2789
75-11#	1.3861	0.0341	0.3446	0.0175	1.2754	1.3998
90-10#	2.0020	0.0178	0.0707	0.0764	1.0466	7.6166

FIGURE 12: A three-dimensional scatter diagram showing brittleness, confining pressure, and bedding angle.

brittleness to plasticity. As the confining pressure increases, the lower the brittleness of the rock and the less prone it is to brittle failure; therefore, this property is often used in engineering practice. If the exposed rock is subjected to confining pressure, e.g., by shotcreting, the possibility of brittle failure by rock bursting can be reduced.

Furthermore, the dispersion of brittleness of slate decreases with the confining pressure increasing.

Confining pressure exerts a significant influence on the brittleness of slate. This is because the energy accumulated at the axial prepeak stage ($W_{mf \cdot A}$) shows significant linear growth with increasing confining pressure, while the residual strain energy at the postpeak stage (W_R) and the work done by the press in the axial postpeak stage ($W_{mb \cdot A}$) show exponential growth with the increase of confining pressure (Figure 14). Substituting $W_{mf \cdot A}$, $W_{mb \cdot A}$, and W_R into

Equation (9), it can be found that the brittleness shows exponential growth with increasing confining pressure.

4.4. Correlation Analysis: Brittleness and Bedding Angle. A fitting curve between brittleness and bedding angle is shown in Figure 15. It can be seen that there is a parabolic relationship between slate brittleness and bedding angle. The brittleness is minimised when the bedding angle is 0°. With increasing bedding angle, the brittleness increases and reaches a maximum when the bedding angle is about 45° and then decreases gradually thereafter. When the bedding angle is 45°, the slate specimen is almost destroyed along the bedding plane according to the Jaeger failure criterion. Due to the weak strength of the bedding plane, the specimen is easily fractured along the bedding plane, showing a relatively
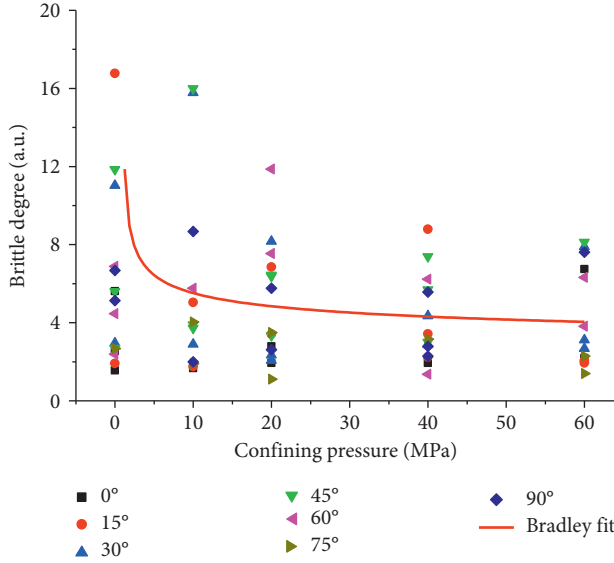
FIGURE 13: Relationship between brittleness and confining pressure.

strong brittleness. In addition, it can be seen from the comparison that the average value of slate brittleness is 4 to 12 under the influence of confining pressure, and 3 to 6 under the influence of bedding angle. This indicated that the confining pressure has a much greater influence on the brittleness of slate than the bedding angle.

Bedding angle has a remarkable influence on the brittleness of slate. It can be seen, from Figure 16(a), that when the bedding angle increases, the energy accumulated at the prepeak stage ($W_{mf \cdot A}$) shows a parabolic relationship whereby it first decreases and then increases; therefore, when the bedding angle is 0° and 90°, the energy accumulated at the axial prepeak stage is larger, while the smallest value occurs at 45°. From Figures 16(b) and 16(c), it can be seen that the residual strain energy at the postpeak stage (W_R) and the work done by the press at the axial postpeak stage ($W_{mb \cdot A}$) show a parabolic relationship, whereby it first increases, and then decreases, with increasing bedding angle; however, the residual strain energy at the postpeak stage is greater when the bedding angle is 90° than when the bedding angle is 0° and vice versa for the work done by press at the axial postpeak stage. Substituting $W_{mf \cdot A}$, $W_{mb \cdot A}$, and W_R into Equation (9), the brittleness has a parabolic relationship whereby it first increases and then declines with increasing bedding angle.

5. Discussion

With the development of rock mechanics, many kinds of brittleness indices have been proposed based on stress-strain curves for different purposes and research objectives; therefore, in this section, the applicability of the index proposed here is illustrated by comparison with five existing brittleness indices.

The typical brittleness indices are as follows:

(1) Br is a brittleness index based on the area under the stress-strain curve

$$Br = \frac{A_1}{A_2}, \tag{10}$$

where A_1 is the area under the line that the slope of it is E_{50} (E_{50} is the deformation modulus at 50% compressive strength), and it passes through the point of peak compressive strength and A_2 is the area under the stress-strain curves.

(2) Br is a brittleness index based on the axial peak strain and the axial residual strain:

$$Br = \frac{(\varepsilon_{A \cdot R} - \varepsilon_{A \cdot P})}{\varepsilon_{A \cdot P}}, \tag{11}$$

where $\varepsilon_{A \cdot P}$ is the axial peak strain and $\varepsilon_{A \cdot R}$ refers to the axial residual strain.

(3) Br is a brittleness index based on compressive strength and residual strength

$$Br = \frac{(\sigma_{A \cdot P} - \sigma_{A \cdot R})}{\varepsilon_{A \cdot P}}, \tag{12}$$

where $\sigma_{A \cdot P}$ is the compressive strength and $\sigma_{A \cdot R}$ is the residual strength.

(4) Br is a brittleness index based on the relative amount, and absolute rate, of stress drop at the postpeak stage

$$Br = \frac{(\sigma_{A \cdot P} - \sigma_{A \cdot R})}{\sigma_{A \cdot P}} \frac{\lg|K_{AC}|}{10}, \tag{13}$$

where $\sigma_{A \cdot P}$ represents compressive strength, $\sigma_{A \cdot R}$ is residual strength, $|K_{AC}|$ is the slope of the line AC where A is the onset of yielding, and C is the residual point of the yield process.

(5) Br is a brittleness index based on peak strain, residual strain, and the residual strength

$$Br = \frac{\varepsilon_{A \cdot R} - \varepsilon_{A \cdot P}}{\varepsilon_{A \cdot P} - \varepsilon_{A \cdot M}}, \tag{14}$$

where $\varepsilon_{A \cdot P}$ is the axial peak strain, $\varepsilon_{A \cdot R}$ represents the axial residual strain, and $\varepsilon_{A \cdot M}$ is the strain at the prepeak stage such that the stress is equal to the residual strength.

It can be seen from Figure 17 that the elastic modulus, peak strength, and residual strength of specimens 30-13 and 60-3 are similar before their peak compressive strength was mobilized. In the earlier stage of the postpeak stage, the stress-strain curves of the specimens are similar: in the postpeak stage, the stress on 30-13 drops at a constant rate, while there are multiple stress-drops seen on specimen 60-3. The mechanical work done by the press, on the two specimens, before their peak strength is similar but there is more energy released from sample 60-3. As a result, the brittleness of specimen 30-13 should be greater than that of 60-3. Therefore, a good brittleness indicator can not only reflect
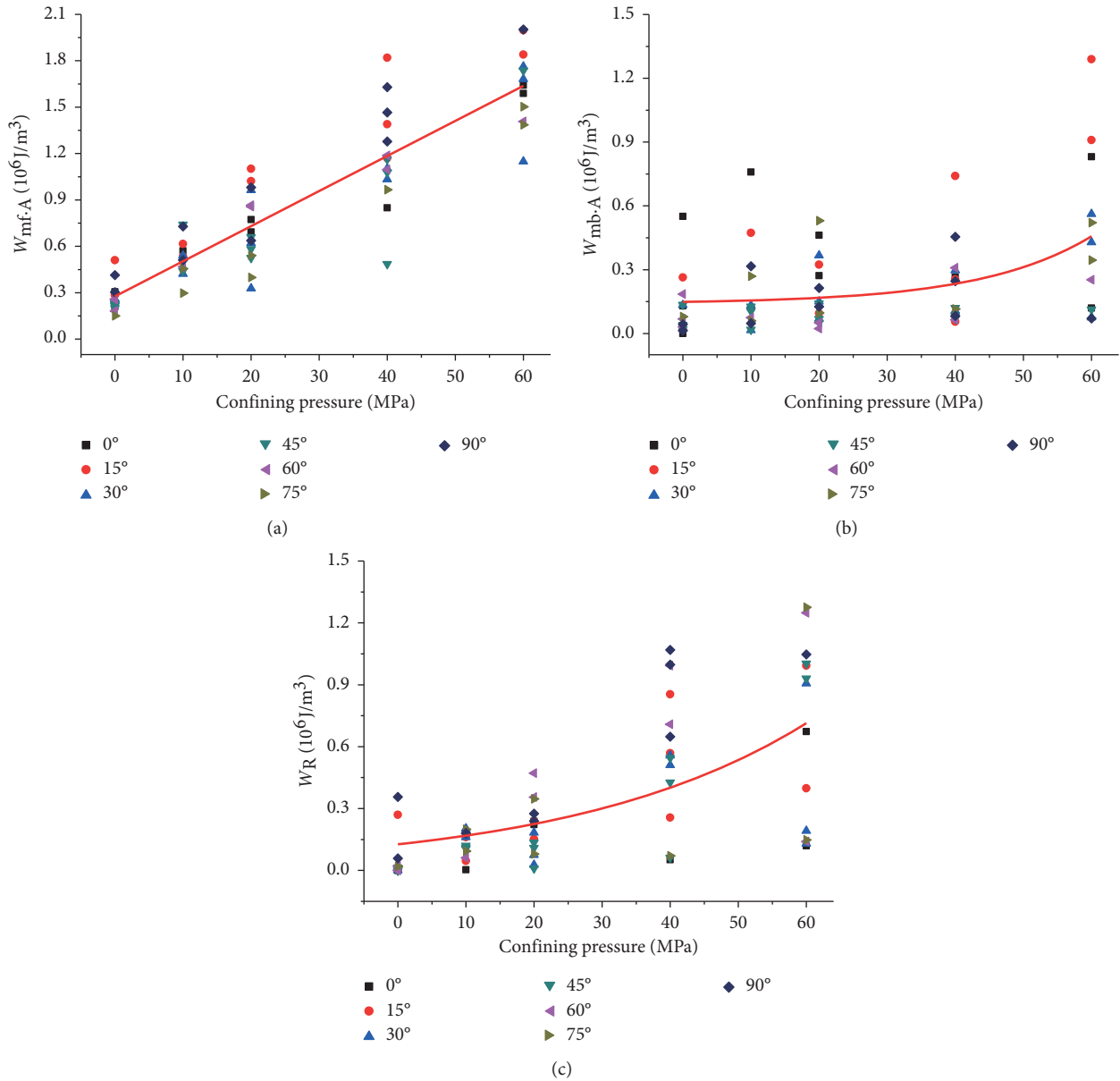
FIGURE 14: Relationship between energy, or work, related to brittleness and confining pressure. (a) The energy accumulated at the axial prepeak stage. (b) The work done by press at the axial postpeak stage. (c) The residual strain energy at the postpeak stage.

the conclusion that brittleness of 30-13 is greater than that of 60-3 in a qualitative sense, but also could distinguish the brittleness of the two specimens quantitatively.

The brittleness values of specimens 30-13 and 60-3 were calculated by using the proposed brittleness index and the five existing brittleness indices mentioned above (Table 2).

It can be seen from Table 2 that the brittleness values of samples 30-13 and 60-3 calculated by the brittleness index proposed by this paper are 2.948 and 2.372, indicating that there is a significant difference between the brittleness of the two specimens. Therefore, the brittleness index proposed by this paper can distinguish the brittleness of the two specimens; however, the brittleness values calculated using the five brittleness indicators mentioned above were very similar. Some results show that the brittleness of sample 30-13 calculated by

the five brittleness indicators is less than that of specimen 60-3. This is contrary to the facts; therefore, the new brittleness index was deemed more suitable for this particular slate.

To investigate the applicability of the five existing brittleness indicators mentioned above for slate, the brittleness of the slate specimens was calculated using the five brittleness indicators. The relationship between the magnitudes of brittleness and confining pressure was obtained and the results are demonstrated in Figure 18.

It can be seen from Figure 18 that the brittleness values of the specimens calculated by different indices all decrease with increasing confining pressure. The conclusion is consistent with the facts as observed experimentally; however, the brittleness values calculated by indices (1), (2), (4), and (5) all decrease within a small range with increasing confining
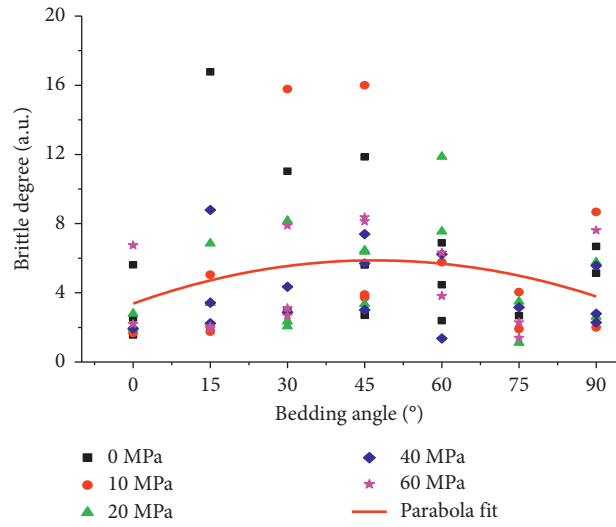
Figure 15: Relationship between brittleness and bedding angle.
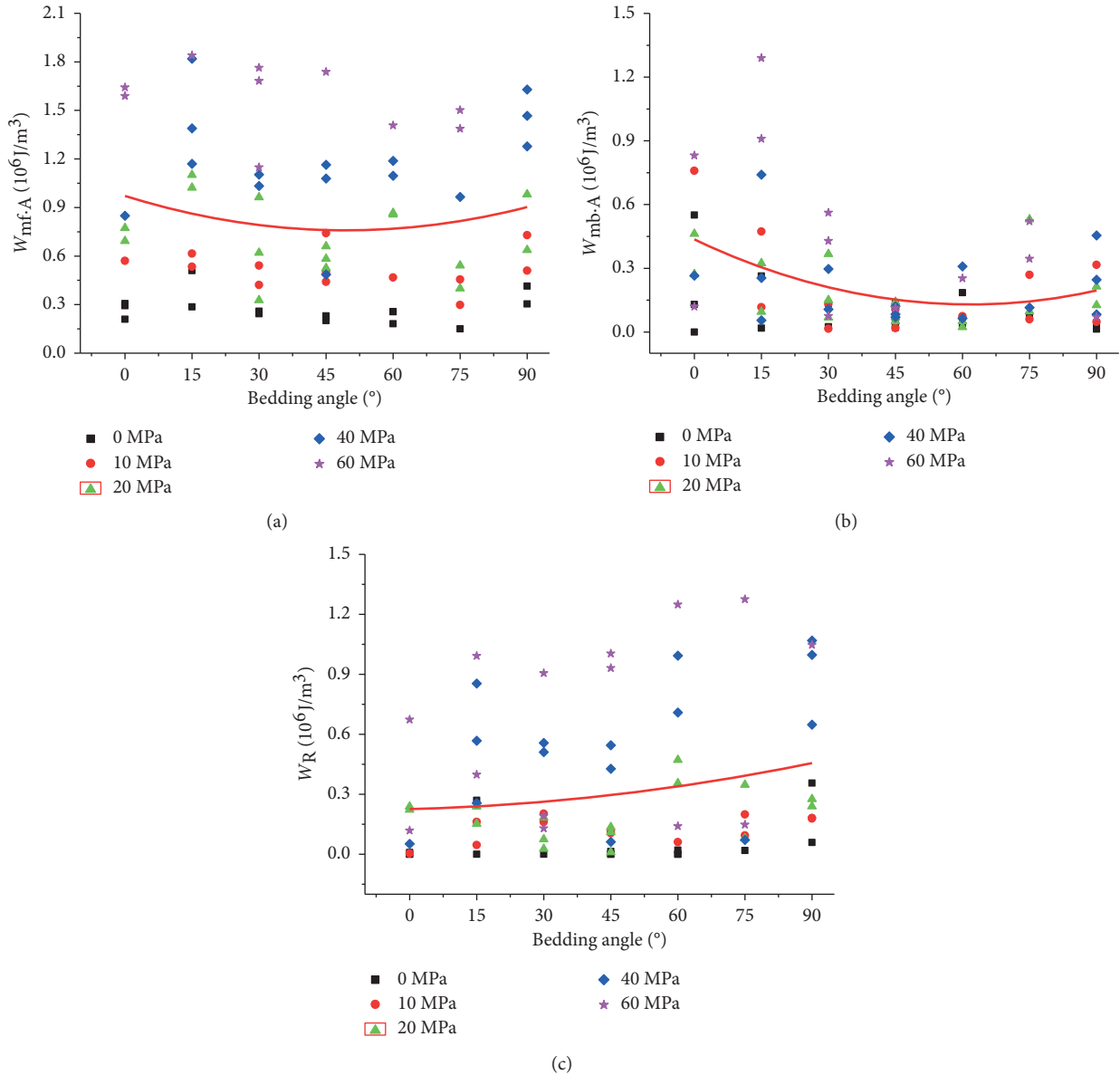

(a)

(b)

(c)

Figure 16: Relationship between energy, or work, related to brittleness and the bedding angle of slate. (a) The energy accumulated at the axial prepeak stage. (b) The work done by press at the axial postpeak stage. (c) The residual strain energy at the postpeak stage.
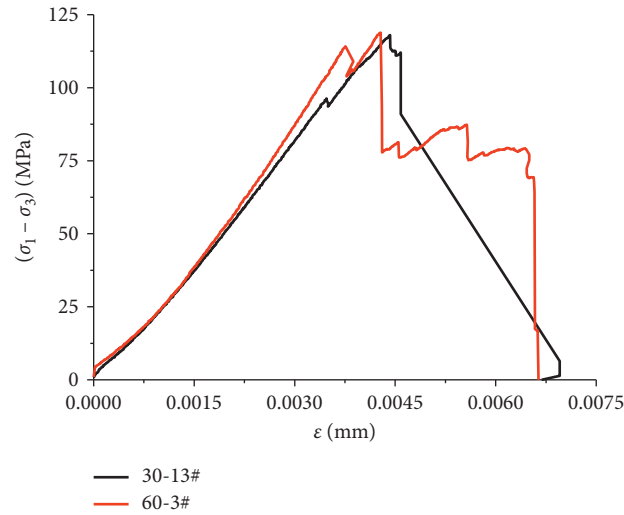
FIGURE 17: Stress-strain curves for specimens 30-13 and 60-3.

TABLE 2: The brittleness of specimens 30-13 and 60-3 under each brittleness index.

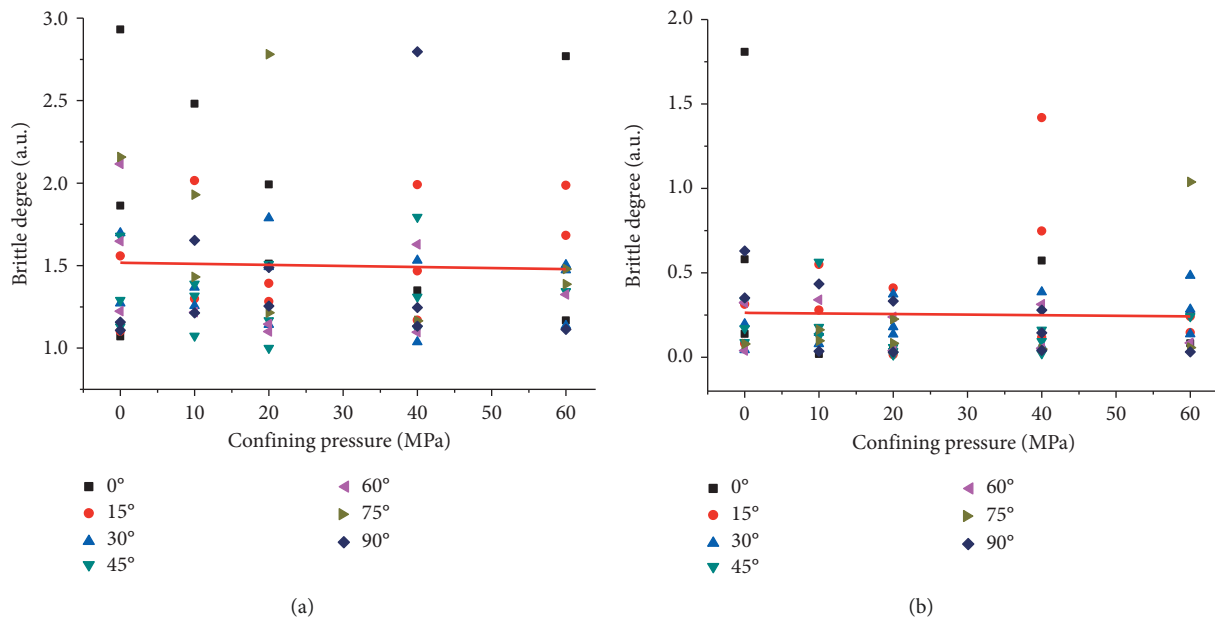|	30-13	60-3
Indices proposed by this paper	2.948737	2.392955
Index (1)	1.696666	2.116477
Index (2)	0.57311	0.550092
Index (3)	0.988135	1
Index (4)	0.164287	0.170261
Index (5)	0.578172	0.550092

(a)

(b)

FIGURE 18: Continued.
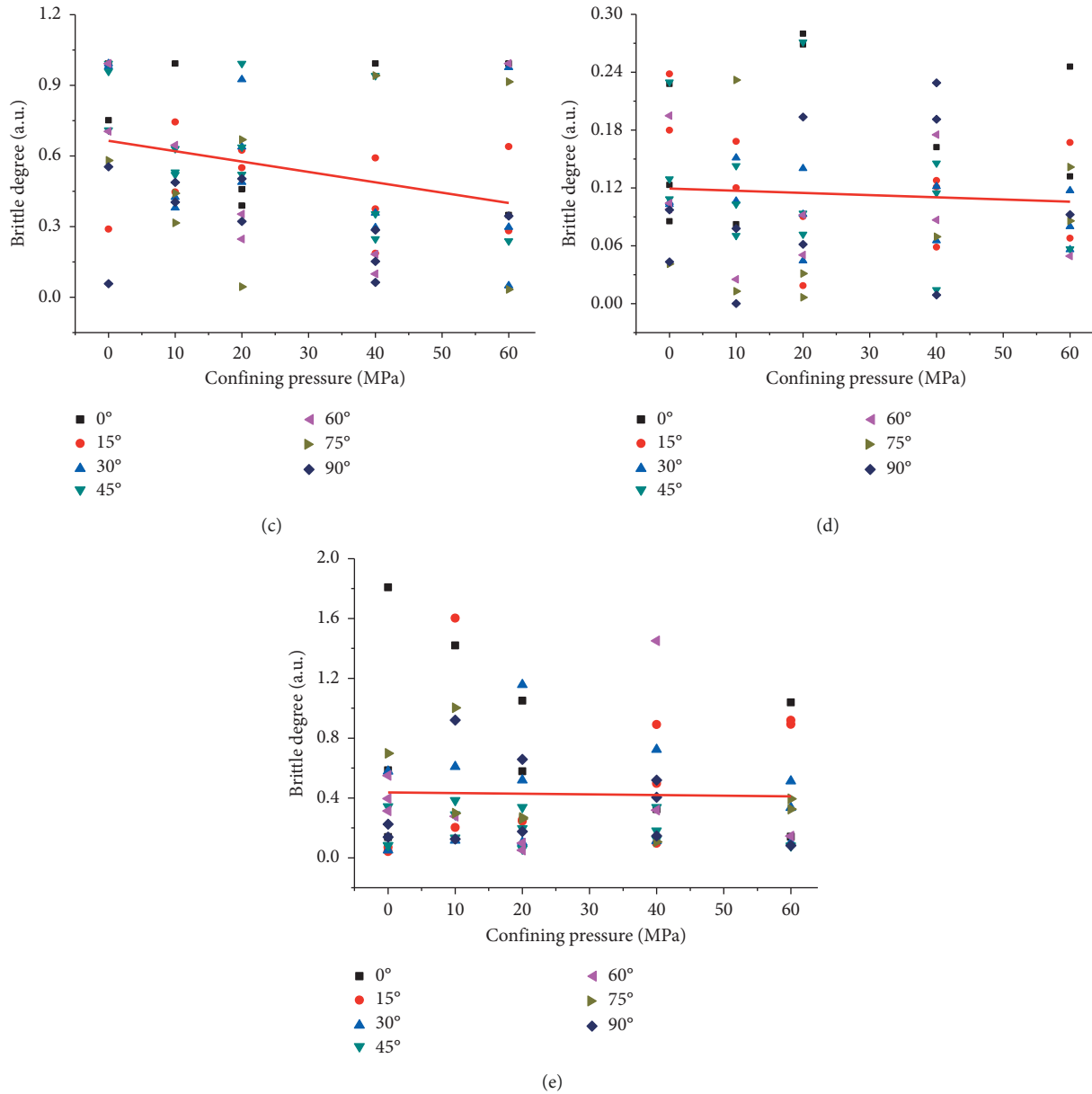
(c)

(d)

(e)

FIGURE 18: Brittleness based on different indices and confining pressures: (a) index (1), (b) index (2), (c) index (3), (d) index (4), and (e) index (5).

pressure, which cannot reflect the effect thereof. For index (3), although effect of the confining pressure on the brittleness calculated by index (3) is obvious, the brittleness values of different specimens under different confining pressures are all within 0 to 1: this indicates insufficient ability of index (3) to distinguish the brittleness of different specimens. The relationship between the brittleness calculated by the brittleness index proposed by this paper and confining pressure is shown in Figure 18: the effect of confining pressure is obvious, and with the increase of confining pressure, the variation in brittleness decreases and the difference between different specimens is obvious.

To sum up, no matter whether it is a reflection of the stress behavior in the postpeak stage of a single specimen, or

the rules of the effect of confining pressure of all specimens, the brittleness index proposed by this paper is more suitable for use on slate samples. This is because most previous indices are based on data at peak compressive strength and residual strength. From the conventional triaxial compression tests of slate (Section 3), it can be seen that the stress-stain curves of slate indicate different types of postpeak behaviors; however, considering only the two points of compressive strength and residual strength, it is difficult to describe the brittleness of slate, for two points cannot reflect the true postpeak behavior with sufficient accuracy. In contrast to the previous indices, the brittleness index based on postpeak energy release proposed in this paper can describe the whole postpeak stage by considering the energy

released in the postpeak stage. Therefore, for rock exhibiting characteristic step-drop, or bench-drop, in the postpeak stage, the brittleness index based on postpeak energy release proposed in this paper is more suitable.

6. Summary and Conclusions

Brittleness is an important indicator of failure in geological materials. The brittleness is an index that could reflect the release rate of energy that accumulated in the slate under the effect of external energy after the peak strength from the perspective of energy. Therefore, a brittleness index based on postpeak energy release for slate was constructed in this paper, which is defined as the increment of dissipated energy released at the postpeak stage divided by the mechanical work done by the press tester after reaching the peak strength. Then conventional triaxial compression tests of 74 specimens were carried out to reveal the effects of confining pressure and bedding angle on the brittleness of slate. The following results were obtained:

(1) The confining pressure exerts a significant influence on the brittleness of slate. With increasing confining pressure, the brittleness of slate shows a rapid decrease. The dispersion of brittleness values of slate decreases with increasing confining pressure.

(2) There is a parabolic relationship between slate brittleness and bedding angle. The brittleness is the smallest when the bedding angle is 0°. With the increase of bedding angle, the brittleness increases and reaches its maximum when the bedding angle is about 45°, and it then decreases gradually thereafter.

(3) Most previous indices are based on data at compressive strength and residual strength points; however, considering only these two points makes it difficult to describe the brittleness of slate, for use of only two points cannot reflect postpeak stage behavior with sufficient accuracy, especially for the rock that undergoes different types of postpeak stress decrease, such as slate.

(4) The brittleness index based on postpeak energy release proposed in this paper can describe the whole of the postpeak stage through an index based on the energy released in the postpeak stage. Therefore, for a rock that exhibits characteristic step-drop, or bench-drop, in its postpeak stage, the brittleness index based on postpeak energy release proposed in this paper is more suitable.

Abbreviations

D: Diameter of specimens
H: Height of specimens
$\varepsilon_{A \cdot P}$: Axial strain of the specimens at the peak strength
σ_P: Compressive strength
$\varepsilon_{A \cdot R}$: Axial strain at the eventual residual stress
$\varepsilon_{C \cdot P}$: Circumferential strain of the specimens at the peak stress
σ_R: Residual strength
$\varepsilon_{C \cdot R}$: Circumferential strain at the eventual residual stress
E: Deformation modulus of the specimens
E_S: Secant modulus
W: Amount of the work done by the external force on the object
ΔU: Amount of the energy change in the object
$W_{mf \cdot A}$: The energy accumulated at the axial prepeak stage
$\Delta U_{sf \cdot A}$: Increment of the axial strain energy at the prepeak stage
V: Volume of the specimens
$S_{(A)}$: Axial stress-strain curve
$S_{(C)}$: Confining stress-strain curve
$W_{mf \cdot C}$: The energy accumulated at the circumferential prepeak stage
$\Delta U_{sf \cdot C}$: Increment of the circumferential strain energy at the prepeak stage
σ_C: Confining pressure
W_{mf}: The energy accumulated at the prepeak stage
$W_{mb \cdot A}$: The work done by press tester at the axial postpeak stage
W_R: Residual strain energy
ΔU_{db}: Increment of dissipation energy released at the postpeak stage
$W_{mb \cdot C}$: The work done by the mechanical press at the circumferential postpeak stage
W_{mb}: The work done by the mechanical press at the postpeak stage
Br: The brittleness of slate
A_1: The area under the line such that its slope is E_{50}
A_2: The area under the stress-strain curves
E_{50}: The deformation modulus at 50% compressive strength
B: Bedding angle
$\varepsilon_{A \cdot M}$: Strain at the prepeak stage that the stress is equal to the residual strength
$Sig.$: Significance
F: F-test value.

Data Availability

The data used to support the findings of this study are included within the article.

Conflicts of Interest

The authors declare that they have no conflicts of interest.

Acknowledgments

References

[1] Q. Sun, L. Xue, and S. Zhu, "Permeability evolution and rock brittle failure," *Acta Geophysica*, vol. 63, no. 4, pp. 978–999, 2015.

[2] M. Sapigni, M. Berti, E. Bethaz, A. Busillo, and G. Cardone, "TBM performance estimation using rock mass classifications," *International Journal of Rock Mechanics and Mining Sciences*, vol. 39, no. 6, pp. 771–788, 2002.

[3] S. Li, X.-T. Feng, Z. Li, C. Zhang, and B. Chen, "Evolution of fractures in the excavation damaged zone of a deeply buried tunnel during TBM construction," *International Journal of Rock Mechanics and Mining Sciences*, vol. 55, pp. 125–138, 2012.

[4] R. Gholami, V. Rasouli, M. Sarmadivaleh, V. Minaeian, and N. Fakhari, "Brittleness of gas shale reservoirs: a case study from the north Perth basin, Australia," *Journal of Natural Gas Science and Engineering*, vol. 33, pp. 1244–1259, 2016.

[5] X. Shi, G. Liu, Y. Cheng et al., "Brittleness index prediction in shale gas reservoirs based on efficient network models," *Journal of Natural Gas Science and Engineering*, vol. 35, pp. 673–685, 2016.

[6] J. Liu, L. Chen, C. Wang et al., "Characterizing the mechanical tensile behavior of Beishan granite with different experimental methods," *International Journal of Rock Mechanics and Mining Sciences*, vol. 69, pp. 50–58, 2014.

[7] X. G. Zhao, M. Cai, J. Wang, and L. K. Ma, "Damage stress and acoustic emission characteristics of the Beishan granite," *International Journal of Rock Mechanics and Mining Sciences*, vol. 64, pp. 258–269, 2013.

[8] X. G. Zhao, J. Wang, M. Cai et al., "Influence of unloading rate on the strainburst characteristics of beishan granite under true-triaxial unloading conditions," *Rock Mechanics and Rock Engineering*, vol. 47, no. 2, pp. 467–483, 2014.

[9] D. R. McCreath and M. S. Diederichs, "Assessment of near-field rock mass fracturing around a potential nuclear fuel waste repository in the Canadian Shield," *International Journal of Rock Mechanics and Mining Sciences & Geomechanics Abstracts*, vol. 31, no. 5, pp. 457–470, 1994.

[10] N. Chandler, "Developing tools for excavation design at Canada's Underground Research Laboratory," *International Journal of Rock Mechanics and Mining Sciences*, vol. 41, no. 8, pp. 1229–1249, 2004.

[11] W. C. Zhu, Z. H. Li, L. Zhu, and C. A. Tang, "Numerical simulation on rockburst of underground opening triggered by dynamic disturbance," *Tunnelling and Underground Space Technology*, vol. 25, no. 5, pp. 587–599, 2010.

[12] X.-T. Feng, Y. Yu, G.-L. Feng, Y.-X. Xiao, B.-r. Chen, and Q. Jiang, "Fractal behaviour of the microseismic energy associated with immediate rockbursts in deep, hard rock tunnels," *Tunnelling and Underground Space Technology*, vol. 51, pp. 98–107, 2016.

[13] M. B. Díaz Aguado and C. González, "Influence of the stress state in a coal bump-prone deep coalbed: a case study," *International Journal of Rock Mechanics and Mining Sciences*, vol. 46, no. 2, pp. 333–345, 2009.

[14] H. Wang, Y. Jiang, S. Xue, X. Pang, Z. Lin, and D. Deng, "Investigation of intrinsic and external factors contributing to the occurrence of coal bumps in the mining area of Western Beijing, China," *Rock Mechanics and Rock Engineering*, vol. 50, no. 4, pp. 1033–1047, 2017.

[15] V. Hucka and B. Das, "Brittleness determination of rocks by different methods," *International Journal of Rock Mechanics and Mining Sciences & Geomechanics Abstracts*, vol. 11, no. 10, pp. 389–392, 1974.

[16] S. Kahraman, "Correlation of TBM and drilling machine performances with rock brittleness," *Engineering Geology*, vol. 65, no. 4, pp. 269–283, 2002.

[17] R. Altindag, "The evaluation of rock brittleness concept on rotary blast hole drills," *Journal of the South African Institute of Mining and Metallurgy*, vol. 102, pp. 61–66, 2002.

[18] R. Altindag, "Correlation of specific energy with rock brittleness concepts on rock cutting," *Journal of the South African Institute of Mining and Metallurgy*, vol. 103, pp. 163–172, 2003.

[19] R. Altindag, "Assessment of some brittleness indexes in rock-drilling efficiency," *Rock Mechanics and Rock Engineering*, vol. 43, no. 3, pp. 361–370, 2010.

[20] C. D. Martin, "Brittle failure of rock materials: test results and constitutive models," *Canadian Geotechnical Journal*, vol. 33, no. 2, p. 378, 1996.

[21] Q. M. Gong and J. Zhao, "Influence of rock brittleness on TBM penetration rate in Singapore granite," *Tunnelling and Underground Space Technology*, vol. 22, no. 3, pp. 317–324, 2007.

[22] Y. J. Xia, L. C. Li, C. A. Tang, X. Y. Li, S. Ma, and M. Li, "A new method to evaluate rock mass brittleness based on stress-strain curves of class I," *Rock Mechanics and Rock Engineering*, vol. 50, no. 5, pp. 1123–1139, 2017.

[23] B. Tarasov and Y. Potvin, "Universal criteria for rock brittleness estimation under triaxial compression," *International Journal of Rock Mechanics and Mining Sciences*, vol. 59, pp. 57–69, 2013.

[24] C. Ai, J. Zhang, Y.-w. Li, J. Zeng, X.-l. Yang, and J.-g. Wang, "Estimation criteria for rock brittleness based on energy analysis during the rupturing process," *Rock Mechanics and Rock Engineering*, vol. 49, no. 12, pp. 4681–4698, 2016.

[25] H. Munoz, A. Taheri, and E. K. Chanda, "Fracture energy-based brittleness index development and brittleness quantification by pre-peak strength parameters in rock uniaxial compression," *Rock Mechanics and Rock Engineering*, vol. 49, no. 12, pp. 4587–4606, 2016a.

[26] H. Munoz, A. Taheri, and E. K. Chanda, "Rock drilling performance evaluation by an energy dissipation based rock brittleness index," *Rock Mechanics and Rock Engineering*, vol. 49, no. 8, pp. 3343–3355, 2016b.

[27] P. K. Kaiser and B.-H. Kim, "Characterization of strength of intact brittle rock considering confinement-dependent failure processes," *Rock Mechanics and Rock Engineering*, vol. 48, no. 1, pp. 107–119, 2015.

[28] J. Li, H. Huang, and M. Wang, "A theoretical derivation of the dilatancy equation for brittle rocks based on Maxwell model," *Acta Geophysica*, vol. 65, no. 1, pp. 1–10, 2017.

[29] P. Lollino and G. F. Andriani, "Role of brittle behaviour of soft calcarenites under low confinement: laboratory observations and numerical investigation," *Rock Mechanics and Rock Engineering*, vol. 50, no. 7, pp. 1863–1882, 2017.

[30] S. Raynaud, D. Ngan-Tillard, J. Desrues, and F. Mazerolle, "Brittle-to-ductile transition in Beaucaire marl from triaxial tests under the CT-scanner," *International Journal of Rock Mechanics and Mining Sciences*, vol. 45, no. 5, pp. 653–671, 2008.

[31] Q. L. Shan, Y. Jin, P. Tan, and R. X. Zhang, "Experimental and numerical investigations on the vertical propagation of hydraulic fractures in laminated shales," *Journal of Geophysics and Engineering*, vol. 15, no. 5, pp. 1729–1742, 2018.

[32] X. Li, C. Qi, Z. Shao, and C. Ma, "Evaluation of strength and failure of brittle rock containing initial cracks under lithospheric conditions," *Acta Geophysica*, vol. 66, no. 2, pp. 141–152, 2018.

[33] M. Heidari, G. R. Khanlari, M. Torabi-Kaveh, S. Kargarian, and S. Saneie, "Effect of porosity on rock brittleness," *Rock Mechanics and Rock Engineering*, vol. 47, no. 2, pp. 785–790, 2014.

[34] H. Fu, J. Zhang, Z. Huang, Y. Shi, and W. Chen, "A statistical model for predicting the triaxial compressive strength of transversely isotropic rocks subjected to freeze-thaw cycling," *Cold Regions Science and Technology*, vol. 145, pp. 237–248, 2018.

[35] H. Wang, T. Yang, and Y. Zuo, "Experimental study on acoustic emission of weakly cemented sandstone considering bedding angle," *Shock and Vibration*, vol. 2018, no. 12, 2018.

[36] J. Liu, Y. Chen, W. Wan, J. Wang, and X. Fan, "The influence of bedding plane orientation on rock breakages in biaxial states," *Theoretical and Applied Fracture Mechanics*, vol. 95, pp. 186–193, 2018.

[37] P.-F. Yin and S.-Q. Yang, "Discrete element modeling of strength and failure behavior of transversely isotropic rock under uniaxial compression," *Journal of the Geological Society of India*, vol. 93, no. 2, pp. 235–246, 2019.

[38] K. Duan, W. Wu, and C. Y. Kwok, "Discrete element modelling of stress-induced instability of directional drilling boreholes in anisotropic rock," *Tunnelling and Underground Space Technology*, vol. 81, no. 55–67, 2018.

[39] Y. Zheng, C. Chen, T. Liu, D. Song, and F. Meng, "Stability analysis of anti-dip bedding rock slopes locally reinforced by rock bolts," *Engineering Geology*, 2019, In press.

[40] X.-J. Hao, L. Yuan, and Y.-X. Zhao, "Influence of initial microcrack on the physic-mechanical properties of rock with slaty cleavage," *Geotechnical and Geological Engineering*, vol. 35, no. 5, pp. 2351–2360, 2017.

[41] S. Q. Yang and W. Y. Xu, "Numerical simulation of strength-size effect of rock materials under different confining pressures," *Journal of Hohai University (Natural Sciences)*, vol. 5, pp. 578–582, 2004.